lized by resonance, such as occurs in benzene. The structures shown in Fig. 5B would normally be found in charge density wave ground states, but instead they are equally contributing resonance structures. Particularly in one dimension, the energy of delocalized systems is usually lowered by distortions. We recently reported the preparation and solid-state characterization of radical **4**, although we were unable to rationalize its electronic structure and properties (*11*). Compound **4** crystallizes as a highly one-dimensional but uniformly spaced π-step structure, and the magnetism may be fit to the antiferromagnetic Heisenberg $S = \frac{1}{2}$ linear chain model (Fig. 5D). Despite its relatively large bandwidth, the absence of a superlattice, and its uniform stacking, compound **4** has σ_{RT} of 1.4×10^{-3} S/cm, and the electronic structure of this compound is best rationalized by the one-dimensional RVB ground state (Fig. 5E). The primary mode of interaction in **5** consists of a linear chain of almost perfectly superimposed π-dimers, in which all of the spin-bearing carbon atoms are in registry. The structure of **4** places neighboring molecules in the stack such that they can only interact through the overlap of one pair of active (spin-bearing) carbon atoms per phenalenyl unit, leading to the π-step structure in which the remaining four active carbon atoms per phenalenyl unit do not interact with their nearest neighbor molecules. In fact, a form of the π-step mode of interaction is also present in **5** (Fig. 1D) and gives rise to the three-dimensional electronic structure of this compound. Nevertheless, in common with lithium (Fig. 4A), in which a number of different interatom electron-pair bonds are possible, compounds **4** and **5** both allow resonance among many pairs of intermolecular (carbon-carbon) bonds.

The structure and properties of compounds **4** and **5** allow us to answer the questions posed by Anderson (*2*). The RVB ground state exists in one (**4**) and three (**5**) dimensions; it is stabilized by resonance and prefers a high-symmetry structure; it conducts electricity but is not a metal; and the excitation spectrum is complex: In the case of **5**, the (band) structure, magnetic susceptibility, conductivity, and electronic spectrum imply different energy gaps (0, 0, 0.11, and 0.34 eV, respectively).

References and Notes

1. L. Pauling, *Nature* **161**, 1019 (1948).
2. P. W. Anderson, *Mater. Res. Bull.* **8**, 153 (1973).
3. P. Fazekas, P. W. Anderson, *Philos. Mag.* **30**, 423 (1974).
4. K. Hirakawa, H. Kadowaki, K. Ubukoshi, *J. Phys. Soc. Jpn.* **54**, 3526 (1985).
5. I. Yamada, K. Ubukoshi, K. Hirakawa, *J. Phys. Soc. Jpn.* **54**, 3571 (1985).
6. P. W. Anderson, *Science* **235**, 1196 (1987).
7. B. J. Powell, R. H. McKenzie, *Phys. Rev. Lett.* **94**, 047004 (2005).
8. X. Chi *et al.*, *J. Am. Chem. Soc.* **121**, 10395 (1999).
9. X. Chi *et al.*, *J. Am. Chem. Soc.* **123**, 4041 (2001).
10. M. E. Itkis, X. Chi, A. W. Cordes, R. C. Haddon, *Science* **296**, 1443 (2002).
11. S. K. Pal *et al.*, *J. Am. Chem. Soc.* **126**, 1478 (2004).
12. Methods and materials are available as supporting material on *Science* Online.
13. K. Goto *et al.*, *J. Am. Chem. Soc.* **121**, 1619 (1999).
14. J. Huang, M. Kertesz, *J. Am. Chem. Soc.* **125**, 13334 (2003).
15. V. Ganesan, S. V. Rosokha, J. K. Kochi, *J. Am. Chem. Soc.* **125**, 2559 (2003).
16. J. Lu, S. V. Rosokha, J. K. Kochi, *J. Am. Chem. Soc.* **125**, 12161 (2003).
17. D. Small *et al.*, *J. Am. Chem. Soc.* **126**, 13850 (2004).
18. R. C. Haddon, A. P. Ramirez, S. H. Glarum, *Adv. Mater.* **6**, 316 (1994).
19. T. Murata *et al.*, *Angew. Chem. Int. Ed. Engl.* **43**, 6343 (2004).
20. R. C. Haddon, S. V. Chichester, J. H. Marshall, *Tetrahedron* **42**, 6293 (1986).

21. Supported by the Office of Basic Energy Sciences, U.S. Department of Energy, under grant no. DE-FG02-04ER46138, and by the U.S. Department of Defense, Defense Advanced Research Projects Agency, Defense Microelectronics Activity under grant no. H94003-04-2-0404.

Supporting Online Material
www.sciencemag.org/cgi/content/full/309/5732/281/DC1
Materials and Methods
Figs. S1 and S2
Tables S1 to S6

18 March 2005; accepted 24 May 2005
10.1126/science.1112446

Penetration of Human-Induced Warming into the World's Oceans

Tim P. Barnett,[1]* David W. Pierce,[1] Krishna M. AchutaRao,[2] Peter J. Gleckler,[2] Benjamin D. Santer,[2] Jonathan M. Gregory,[3] Warren M. Washington[4]

A warming signal has penetrated into the world's oceans over the past 40 years. The signal is complex, with a vertical structure that varies widely by ocean; it cannot be explained by natural internal climate variability or solar and volcanic forcing, but is well simulated by two anthropogenically forced climate models. We conclude that it is of human origin, a conclusion robust to observational sampling and model differences. Changes in advection combine with surface forcing to give the overall warming pattern. The implications of this study suggest that society needs to seriously consider model predictions of future climate change.

Wide-ranging evidence shows that Earth has been warming in recent decades (*1*). Observations show that ~84% of the total heating of the Earth system (oceans, atmosphere, continents, and cryosphere) over the last 40 years has gone into warming the oceans (*2*). Therefore, if one wishes to understand and explain this warming, the oceans are clearly the place to look.

There have been only a few studies that have tried to both detect (i.e., differentiate from expected natural variability) and attribute (i.e., ascribe a cause to) the observed ocean warming signal (*3*–*8*). All used the equivalent of a single ocean-basin temperature measure and tracked its change with time. This approach neglects information on how the warming penetrates vertically into the ocean, and variations of the penetration from basin to basin. The studies all suggest human impacts on the oceans, but some did not consider the possibility that the observed warming was due to natural external forcing such as solar variability or volcanic activity.

Here we investigate the warming since 1960 on an ocean-by-ocean basis and focus on how the signal penetrates down into the ocean. We use a recently upgraded and much expanded observed ocean data set (*2*), which provides the best available description of the ocean's warming signal and its evolution through time. In addition to examining these observational data, we compare them to simulations from two independent climate models, the Parallel Climate Model (PCM) (*9*) and the Hadley Centre model (HadCM3) (*10*). We then use the results of numerical experiments with these models to attribute the causes of the observed warming. The models allow gross heat budgets to be constructed by basin; these show that changes in net surface heat flux combine with advection at depth to give the observed signal.

We first define a model-based "fingerprint" describing the warming signal at each vertical level using the geographical and temporal variability of ocean temperature (*11*). The observations, projected onto this fingerprint at each level, show that the strength of the warming signal varies from ocean to ocean (*11*) (Fig. 1). The warming extends to depths of

[1]Climate Research Division, Scripps Institution of Oceanography, 0224, La Jolla, CA 92037, USA. [2]Program for Climate Model Diagnoses and Intercomparison/Lawrence Livermore National Laboratory, Post Office Box 808, Livermore, CA 94550, USA. [3]UK Met Office Hadley Centre and University of Reading, Reading RG6 6BB, UK. [4]National Center for Atmospheric Research, Post Office Box 3000, Boulder, CO 80307, USA.

*To whom correspondence should be addressed. E-mail: tbarnett@ucsd.edu

700 m or more in both the North and South Atlantic oceans, but is largely confined to the upper 100 m of the northern Pacific and northern Indian oceans. The northern Indian Ocean is particularly unusual in that it has a subsurface maximum. Both the northern and southern Pacific Ocean show a sign reversal in the warming signals, indicating a cooling at ~150-m depth. These differences between oceans constitute the spatial structure of the warming fingerprint. The final dimension of the signal is the temporal evolution of the differences. Because we are interested in low-frequency variations, we use decadal time averages to describe this time evolution.

Our purpose is to understand the origin of this complex time- and space-dependent signal. We explore three possible causes: natural variability internal to the coupled ocean-atmosphere system; external natural variability, such as solar or volcanic forcing; and forcing arising from human activity [emission of greenhouse gases (GHGs) and sulfate aerosols].

The likelihood that natural internal climate variability is the cause of the observed warming signal can be examined by analyzing a long control run of the PCM; i.e., how well did natural internal variability in the control run project onto the warming fingerprint (*11*)? This approach was used in earlier work (*3*) and is a variant of standard detection and attribution analysis (*12*–*15*). It has the advantage of having a simple geometric explanation while being rigorous in a statistical sense (*11*).

The strength of the warming signal in the control run (sampled in the same places as the observations) is shown in Fig. 2 for each ocean. This gives some indication of the fluctuations in signal strength that one might expect due to natural internal variability alone. Because we had multiple realizations of the 40-year time period in the control runs, we can show the 90% confidence limits of the natural variability by the hatched region. Also shown is the signal strength in the observations (red dots) from Fig. 1. The illustration demonstrates that the warming signal is far stronger than would be expected from natural internal variability, as estimated by the model. To assess whether the model's estimate of natural variability is reasonable, we compared the levels of variance in the control run at decadal time scales to those observed and found that they matched reasonably well (*16*) (supporting online text). Therefore, the control run variations are a reasonable representation of natural internal variability, at least on the decadal time scales of interest here.

Another possible candidate for the warming signal is natural variability external to the ocean-atmosphere system, such as solar variability or volcanic eruptions ("SV" forcing). We explored this possibility by analyzing PCM runs forced by estimates of observed solar variability and volcanic aerosol loadings (*17*). The results of four such runs were combined and the warming signal strength estimated in the SV data set. The results (Fig. 2) show that in none of the oceans can the SV forcing (green triangles) replicate the observed warming. Indeed, at these space and time scales, the SV forcing produces signal strengths indistinguishable from those expected from natural internal variability (hatched region).

The final candidate for explaining the signal is anthropogenic factors, such as well-mixed GHGs and sulfate aerosol particles. We examined this possibility in an ensemble of

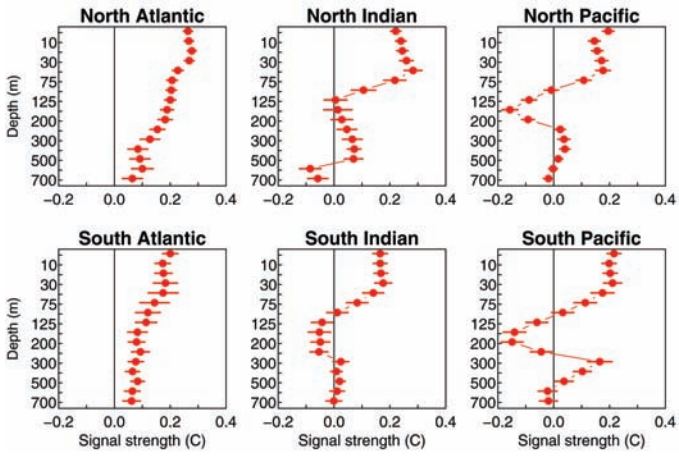

Fig. 1. Warming signal strength by ocean and depth. The dots represent the projection of the observed temperature changes onto the model-based pattern of warming. They show substantial basin-to-basin differences in how the oceans have warmed over the past 40 years, although all oceans have experienced net warming over that interval. The horizontal bars represent the ±2SD limits associated with sampling uncertainty.

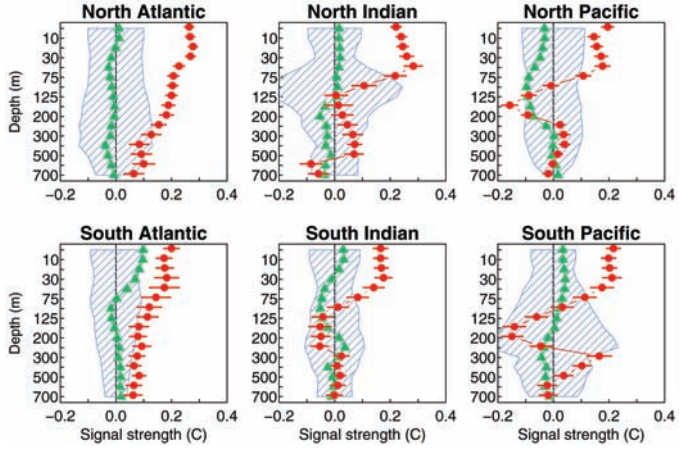

Fig. 2. Multiple realizations from the PCM control run allowed estimation of the probability distribution of signal strength associated with natural internal variability. The hatched region represents the 90% confidence limits of the natural internal variability signal strength. The observed signal strength (red dots) bears little resemblance to that expected from natural internal variability. The ensemble-averaged strength of the warming signal in four runs forced by observed solar and volcanic variability (green triangles) is also shown. There is no agreement between the two. The solar plus volcanic signals are generally indistinguishable from those expected from natural internal variability alone on the time and space scales used in this study.

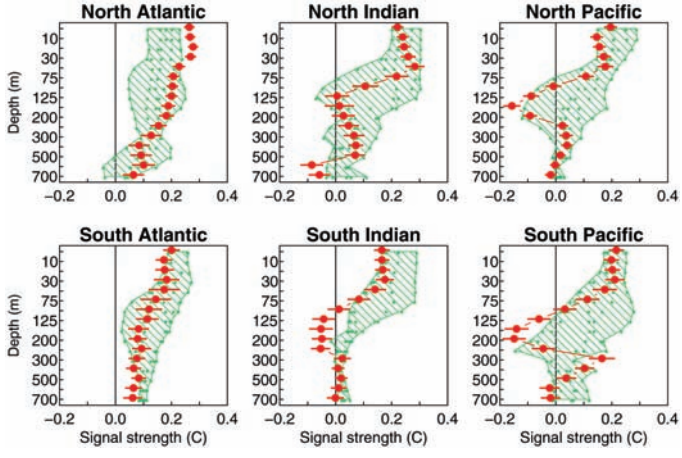

Fig. 3. Anthropogenic forcing signal strength (green hatched region) compared to that obtained from the observations (red dots). There is excellent agreement at most depths in all oceans. The hatched region shows the range of the signal strength estimates from five different realizations of identically forced simulation with the PCM, whereas the smaller green dots within the region are the individual realizations.

five PCM runs with such forcing (*17*, *18*). The results (Fig. 3) show the range of the signal strength in five scenario runs by ocean and depth (hatched area) in comparison with the observations (red dots). An ocean-by-ocean and depth-by-depth comparison shows that the agreement is compelling. The immediate conclusion is that human influences are largely responsible for the warming signal. This level of agreement could not have been tuned into the models, because the fingerprint is too complex in space and time. Further, about half of the observations used in this study were not available when the computer simulations were run.

The different response of individual oceans to GHG forcing is an interesting finding. The physical reasons for this are fairly well known, with one major surprise. For instance, it is well known that deep convection is characteristic of both the North and South Atlantic oceans (*19*). That explains why the warming signal penetrates relatively deeply in these oceans. In contrast, the northern Pacific Ocean is characterized by a rather shallow meridional overturning circulation (*20*) that tends to isolate the surface layers from the deeper ocean. It is also true that no deep water is formed in the northern Pacific. Both physical properties act to confine the signal to the upper ocean. The same situation is thought to hold over much of the southern Indian Ocean.

One notable feature from the observed and modeled signal strength (Figs. 1 and 3) is the negative lobe at 150- to 200-m depth in the Pacific. The simulation that captured this signal showed that it is associated with a thinning of the western Pacific warm pool associated with shoaling of the deeper isotherms, which has also been observed in the Pacific since the 1970s (*20*).

The major surprise is the northern Indian Ocean, which has rather shallow signal penetration and a subsurface maximum in signal strength. The heat budget for this region (Fig. 4) shows that it is the only basin where the ensemble variability includes zero for the net surface heat flux, and where advective warming is the dominant cause of the basin temperature change over the last 60 years in PCM. This result is likely due to the cancellation of GHG warming by sulfate aerosol cooling, a result recently found from direct observations (*21*). Further simulations have shown that carbon aerosols also play a role in this effect (*22*), but are not included in the simulations of this paper. Hence the warming of this ocean over the past 60 years in the simulation was largely due to changes in advection. Recent observations show a slowing of the shallow meridional circulation cell in the Indian Ocean such that advection from northern to southern Indian Ocean is reduced, leading to a net warming of the northern Indian Ocean (*23*), a result in accord with the model predictions. Indeed, inspection of the partition of net surface air/sea heat exchange and advection for the various oceans (Fig. 4) shows that in several basins, changes in advection of heat by ocean currents redistribute the heat gained from the anthropogenic forcing, and so are important to determining the structure and evolution of the warming signal in the oceans [compare (*7*)].

The normalization by surface area used in Fig. 4 removes the geometric impact of ocean size on our results. It also makes clear that the southern oceans are absorbing more heat per unit area than are the northern oceans. We suggest that this is again due to the smaller aerosol concentrations over the southern oceans. They do not have the same near-canceling effects observed in the more polluted Northern Hemisphere (*21*, *22*).

Is PCM unique in being able to capture the complex observed signal? To address this question, we repeated the analysis with HadCM3, which was developed at the Hadley Centre independently of PCM. The four realizations from this model were the "All" forcings runs, which combined a variety of forcings [GHG, solar, volcanic, aerosols, etc. (*24*)]. HadCM3's warming fingerprint (not shown) is little different from PCM's, but we use exclusively PCM's fingerprint here for consistency. The results from HadCM3 are compared to observations in Fig. 5. Using the HadCM3 fingerprint gives even better agreement (not shown), as one would expect. In any event, Figs. 3 and 5 show that PCM and HadCM3 both reflect reasonably well the evolution and spatial characteristics of the warming signal.

An interesting feature of the above result is that the PCM and HadCM3 are very different models. In the simulations used here, their forcings are also rather different. How could they give very similar evolutions of ocean temperature? Whatever the combinations of forcing used by the two modeling groups, the net forcing at the surface of the ocean had to be essentially the same. Inspection of each model's surface heat flux fields, in so far as possible, shows this to be the case. The details of the atmospheric forcing and climate feedbacks that go into producing that net value do not affect the overall oceanic response. The story may be different in the atmosphere.

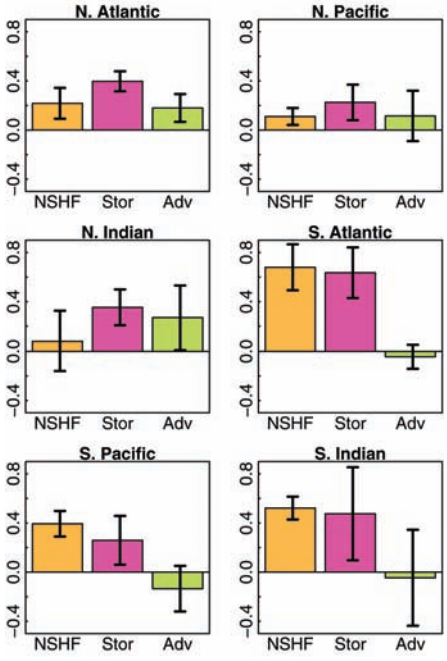

Fig. 4. Gross heat budget by ocean showing the important role that heat advection by ocean currents plays in the anthropogenic warming of the world's oceans. The PCM's net ocean surface heat flux averaged over 1940 to 1999 is shown by the "NSHF" bars, the modeled changes in ocean basin heat storage by the "Stor" bars, and the advection of heat by ocean currents needed to close the heat budget by the "Adv" bars. The latter was obtained as a residual from the first two estimates. The uncertainty bars indicate ±1SD based on the ensemble spread. The actual energy change (joules) over the time period has been normalized by surface area of respective oceans to give the average heating rate in W/m^2. This normalization makes it appear that the net advection over the globe is nonzero, a condition that vanishes using the area-weighted fluxes.

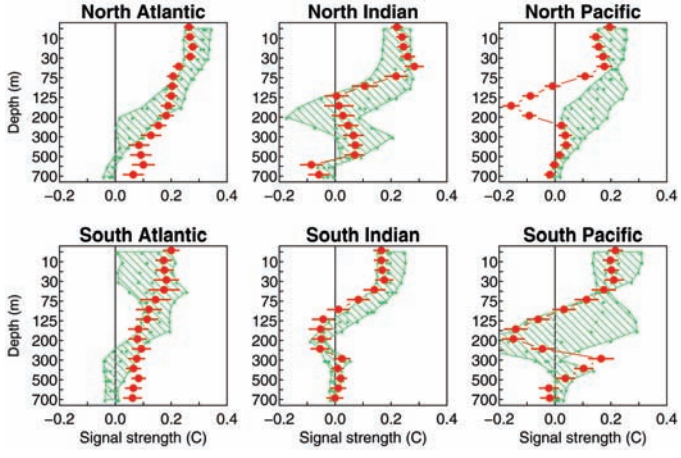

Fig. 5. Comparison of the model-predicted anthropogenic signals between HadCM3 and observations for the oceans. The format is described in Fig. 3. Comparison of Figs. 3 and 5 shows that both models capture the main structure of the signal in the observations. These figures were derived by using the warming signal defined by PCM as the basis set to allow a consistent comparison.

It is also important to investigate the influence of the upgraded data set (*2*), sampling, and model uncertainties on our conclusions. In all our results, we use a sampling strategy that compares model and observations only where observations exist; we do not use the infilled or interpolated data set (*11*). As a test, however, we repeated the analysis using the infilled data and found that it made no difference to the conclusions. More details on these sampling issues are found in (*16*). We also estimated the impact that model errors might have on the results. Multiple models run with the same GHG forcing (*25*) show a factor of 2 difference in ocean basin heat content after 80 years of integration (*26*, *27*). We estimated the effect that this had in the detection scheme and still found robust detection results above the level of natural variability (*16*). Therefore, the conclusion that the observed ocean warming is due to human influences is robust to major perturbations of both the observed data set and model error.

The implications of our results go far beyond identifying the reasons for ocean warming. First, they show that uncertainties in the models used here are too small to affect the conclusion attributing the historic ocean warming signal to anthropogenic forcings, at least for the temperature-driven part of the signal. Second, taking these new results with those obtained in the last few years [e.g., (*1*, *28*–*30*); see earlier detection studies cited above] leaves little doubt that there is a human-induced signal in the environment. Third, because the historical changes have been well simulated, future changes predicted by these global models are apt to be reasonably good, at least out to, say, 20 to 30 years into the future. How to respond to the serious problems posed by these predictions is a question that society must decide.

References and Notes

1. IPCC, "WG1 Third Assessment Report," J. T. Houghton *et al.* Eds. (2001).
2. S. Levitus, J. Antonov, T. Boyer, *Geophys. Res. Lett.* **32**, L02604, doi:10.1029/2004GL021592 (2005).
3. T. P. Barnett, D. W. Pierce, R. Schnur, *Science* **292**, 270 (2001).
4. S. Levitus *et al.*, *Science* **292**, 267 (2001).
5. B. K. Reichert, R. Schnur, L. Bengtsson, *Geophys. Res. Lett.* **29**, 1525 (2002).
6. J. Hansen *et al.*, *J. Geophys. Res.* **107** (D18), 4347 (2002).
7. J. M. Gregory, H. T. Banks, P. A. Stott, J. A. Lowe, M. D. Palmer, *Geophys. Res. Lett.* **31**, L15312 (2004).
8. P. R. Gent, G. Danabasoglu, *J. Clim.* **17**, 4058 (2004).
9. W. M. Washington *et al.*, *Clim. Dyn.* **16**, 755 (2000).
10. C. Gordon *et al.*, *Clim. Dyn.* **16**, 147 (2000).
11. Methods are available as supporting material on *Science* Online.
12. G. C. Hegerl *et al.*, *J. Clim.* **9**, 2281 (1996).
13. G. C. Hegerl *et al.*, *Clim. Dyn.* **13**, 613 (1997).
14. M. R. Allen, S. F. B. Tett, *Clim. Dyn.* **15**, 419 (1999).
15. K. Hasselmann, *Clim. Dyn.* **13**, 601 (1997).
16. D. W. Pierce *et al.*, in preparation.
17. G. A. Meehl, W. M. Washington, T. M. L. Wigley, J. M. Arblaster, A. Dai, *J. Clim.* **16**, 426 (2003).
18. A. Dai, W. M. Washington, G. A. Meehl, T. W. Bettge, W. G. Strand, *Clim. Change* **62**, 29 (2004).
19. G. Neumann, W. J. Pierson, *Principles of Physical Oceanography* (Prentice-Hall, NJ, 1966).
20. M. J. McPhaden, D. Zhang, *Nature* **415**, 603 (2002).
21. V. Ramanathan *et al.*, *J. Geophys. Res.* **106**, 28,371 (2001).
22. V. Ramanathan *et al.*, in preparation.
23. T. Lee, *Geophys. Res. Lett.* **31**, L18305 (2004).
24. S. F. B. Tett, P. A. Stott, M. R. Allen, W. J. Ingram, J. F. B. Mitchell, *Nature* **399**, 569 (1999).
25. CMIP2+ runs are available at http://www-pcmdi.llnl.gov.
26. A. P. Sokolov, C. E. Forest, P. H. Stone, *J. Clim.* **16**, 1573 (2003).
27. K. M. AchutaRao *et al.*, in preparation.
28. B. D. Santer *et al.*, *Science* **301**, 479 (2003).
29. B. D. Santer *et al.*, *J. Geophys. Res.* **109**, D21104 (2004).
30. B. D. Santer, J. E. Penner, P. W. Thorne, in *Temperature Trends in the Lower Atmosphere: Steps for Understanding and Reconciling Differences* (Report by the U.S. Climate Change Science Plan and the Subcommittee on Global Change Research, Washington, DC, in press).

31. This work is a contribution from the International Detection and Attribution Group funded by the National Oceanic and Atmospheric Association (NOAA) and the U.S. Department of Energy (DOE) through NOAA's CCDD program. We gratefully acknowledge DOE support through grants DE-FG03-01ER63255 to the Scripps Institute of Oceanography and DOE-W-7405-ENG-48 to the Program for Climate Model Diagnoses and Intercomparison at Lawrence Livermore National Labatory. Work at the Hadley Centre was supported by the UK Department for Environment, Food and Rural Affairs under contract PECD 7/12/37 and by the Government Meteorological Research and Development Programme. We especially thank S. Levitus for making his new ocean data set available and colleagues at NCAR and the Hadley Centre for performing and making available the model runs used in this work. Computer time for the PCM simulations was provided by the National Center for Atmospheric Research Scientific Computing Division, the DOE National Energy Research Scientific Computing Center, Oak Ridge National Laboratory, and the Los Alamos National Laboratory's Advanced Computing Laboratory. Discussions with L. Talley and R. Davis were helpful in several aspects of the study.

Supporting Online Material

www.sciencemag.org/cgi/content/full/1112418/DC1
Materials and Methods
SOM Text
Figs. S1 and S2
References and Notes

17 March 2005; accepted 12 May 2005
Published online 2 June 2005;
10.1126/science.1112418
Include this information when citing this paper.

Ecosystem Collapse in Pleistocene Australia and a Human Role in Megafaunal Extinction

Gifford H. Miller,[1] Marilyn L. Fogel,[2] John W. Magee,[3] Michael K. Gagan,[4] Simon J. Clarke,[5] Beverly J. Johnson[6]

Most of Australia's largest mammals became extinct 50,000 to 45,000 years ago, shortly after humans colonized the continent. Without exceptional climate change at that time, a human cause is inferred, but a mechanism remains elusive. A 140,000-year record of dietary $\delta^{13}C$ documents a permanent reduction in food sources available to the Australian emu, beginning about the time of human colonization; a change replicated at three widely separated sites and in the marsupial wombat. We speculate that human firing of landscapes rapidly converted a drought-adapted mosaic of trees, shrubs, and nutritious grasslands to the modern fire-adapted desert scrub. Animals that could adapt survived; those that could not, became extinct.

Humans are thought to have colonized Australia between 55 and 45 thousand years ago (ka) (*1*–*5*), and most of its large animals became extinct between 50 and 45 ka (*6*, *7*). The 60 taxa known to have become extinct include all large browsers, whereas large grazing forms, such as red and gray kangaroos, were less affected. The selective loss of large browse-dependent taxa suggests that ecosystem change may have been important, although animal size may have played a role (*8*). Inferential evidence of vegetation reorganization and a changed fire regime beginning 45 ka is recorded in terrestrial (*9*, *10*) and marine (*11*, *12*) sediment cores. But no records of ecosystem status through this time interval are available from the vast semiarid zone. We used isotopic tracers of diet preserved in avian eggshells and marsupial teeth (*13*, *14*) to monitor ecosystems before and after human colonization. These dietary reconstructions document ecosystem collapse across the semiarid zone between 50 and 45 ka.

We recovered eggshells of the Australian emu *Dromaius novaehollandiae* and the extinct giant flightless bird *Genyornis newtoni* from longitudinal desert dunes and shoreline-

[1]INSTAAR and Geological Sciences, University of Colorado, Boulder, CO 80309–0450 USA. [2]Geophysical Laboratory, Carnegie Institution of Washington, 1051 Broad Branch Road, Washington, DC 20015, USA. [3]Department of Earth and Marine Sciences, [4]Research School of Earth Sciences, Australian National University, Canberra, ACT 0200, Australia. [5]Charles Sturt University, Locked Bag 588, Wagga Wagga, NSW 2678, Australia. [6]Department of Geology, Bates College, Lewiston, ME 04240–6028, USA.